Dimethylaniline-tetracyanobutadiene and dimethylaniline-extended-tetracyanobutadiene functionalized BODIPYs witnessing ultrafast charge transfer

Indresh S. Yadav,[a ‡] Ram R. Kaswan,[b ‡] Anuradha Liyanage,[b ‡] Rajneesh Misra*[a] and Francis D'Souza, *[b]

[a] Department of Chemistry, Indian Institute of Technology Indore, Indore 453552, India

E-mail: rajneeshmisra@iiti.ac.in

[b] Department of Chemistry, University of North Texas at Denton, 1155 Union Circle, #305070, Denton, TX 76203-5017 (USA)

E-mail: Francis.Dsouza@unt.edu

[‡] *Equal contributions*

ABSTRACT

A new series of donor-acceptor push-pull systems, **BODIPYs 1–4** were designed and synthesized by the palladium-catalyzed Sonogashira cross-coupling and [2+2] cycloaddition-retroelectrocyclization reactions in good yields. To prepare **BODIPY 3** and **4**, **BODIPY 2** was modified with strong electron acceptors, tetracyanoethylene (TCNE) and 7,7,8,8-tetracyanoquinodimethane (TCNQ), resulting in tetracyanobutadiene (TCBD) and cyclohexa-2,5-diene-1,4-diylidene-expanded-TCBD (DCNQ) functionalized **BODIPY 3** and **4**, respectively. The effect of electron donor *N, N*-dimethylaniline (NND), and acceptors, TCBD and DCNQ on the photophysical and redox properties of the BODIPYs are explored. The push–pull **BODIPYs 1–4** exhibit ICT band at longer wavelengths due to strong D–A interactions. The redox properties of the **BODIPYs 1–4** exhibit multiple-redox waves due to redox-active NND, BODIPY, TCBD, and DCNQ moieties. The computational studies were performed at the B3LYP/6-31G (d,p) level to understand the molecular geometry and electronic structure of the push-pull BODIPYs. The incorporation of a strong acceptor, the DCNQ decreased the LUMO levels more than the TCBD unit. The femtosecond pump-probe studies were performed to witness the excited state charge separation process in dichlorobenzene for the **BODIPYs 1–4**. Finally, the data was analyzed by global target analysis (GloTarAn) which revealed the lifetime of charge-separated states in the range of 45–160 ps in dichlorobenzene, signifying their potential use in energy harvesting and other optoelectronic applications.

INTRODUCTION

The π-conjugated push-pull molecular systems have gained considerable interest in the scientific community due to their tunable optoelectronic properties and wide range of applications such as in organic field-effect transistors, non-linear optics, photovoltaic devices, energy harvesting, bio-imaging, sensors, organic light-emitting diodes.[1-9] The optoelectronic properties and HOMO–LUMO gap of the π-conjugated chromophores can be altered by modifying the donor (D) or acceptor (A) unit or the π-linker between the D and A unit.[10,11] The 4,4-difluoro-4-bora-3a,4a-diaza-*s*-indacene dyes, frequently known as BODIPY have attracted a lot of attention in the last few decades because of their excellent chemical and photophysical properties including strong absorption, high fluorescence quantum yields and molar absorption coefficients, low toxicity, long fluorescence lifetime as well as good photochemical stability.[12–20] The optoelectronic characteristics of the BODIPYs can be tuned by expanding the conjugation and incorporation of appropriate D/A groups at the *meso* and pyrrolic locations (α and β–positions).[21–25] As a result, the BODIPY-based π-conjugated dyes have been extensively used in building fluorescent imaging agents, molecular switches, chemosensors, laser dyes, light-emitting devices, photosensitizers, and optoelectronic materials.[26–31] Noticeably, depending upon the peripheral substituents the BODIPY unit can act as an electron donor or acceptor.[32-34]

The [2+2] cycloaddition-retroelectrocyclization is a catalyst-free reaction known for good reaction yields.[35] In this reaction, the electron-rich alkynes react with the strong acceptors, TCNE and TCNQ, resulting in the nonplanar push-pull molecules with low HOMO–LUMO gaps.[36–38] The push-pull molecular systems based on TCBD and DCNQ exhibit strong intramolecular charge transfer (ICT) revealing new optical transitions at higher wavelengths.[35,39,40] Consequently, the TCBD and DCNQ-carrying push-pull systems have emerged as potential candidates in optoelectronics.[41,42] Diederich, Michinobu, Shoji, Trolez, and Butenschön *et al.* have explored the synthesis, photophysical, and redox properties of TCBD and DCNQ functionalized push-pull chromophores as redox-active ICT systems for optoelectronic applications.[43–48] Recently, our groups reported the TCBD and DCNQ functionalized push-pull systems and explored their photophysical and redox properties for optoelectronic applications.[49]

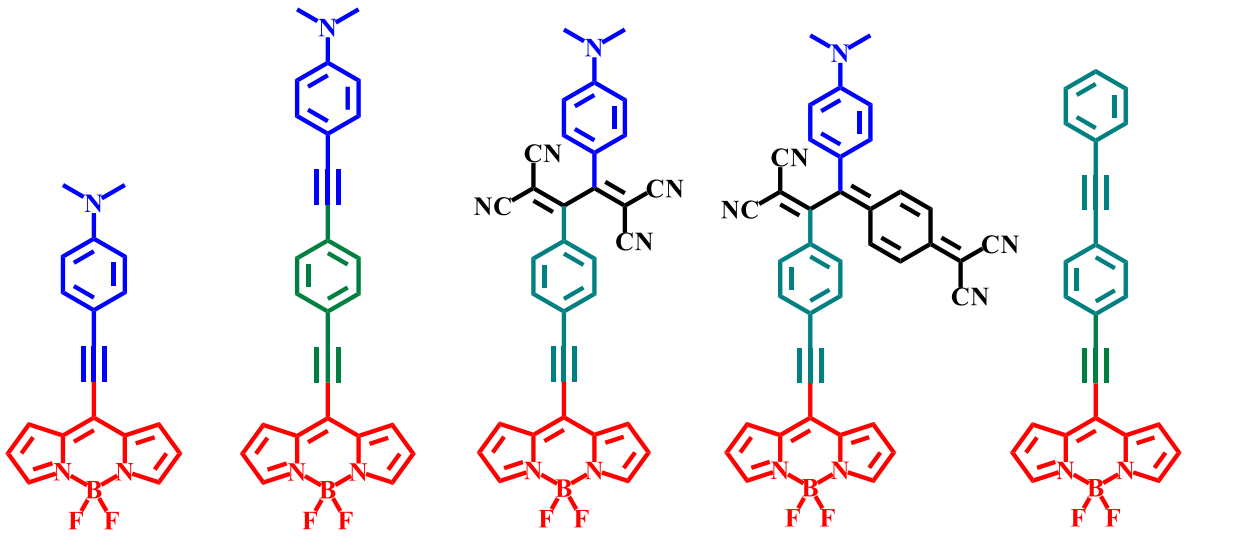

Chart 1. Molecular structures of the push-pull **BODIPYs 1–4** and control compound **C1**.

In the present contribution, we wish to report push-pull **1–4** that are synthesized by the palladium-catalyzed Sonogashira cross-coupling and [2+2] cycloaddition-retroelectrocyclization reactions in good yields. As demonstrated here, the TCBD and DCNQ substituted **3** and **4** exhibit ICT bands at a longer wavelength due to strong D–A interactions. The redox properties of the push-pull **3** and **4** exhibit facile reductions due to the strong electron acceptor nature of TCBD and DCNQ. Additionally, theoretical studies are carried out to analyze the molecular geometry and push-pull contributions of different entities in **1–4**. Ultrafast charge separation has been observed in these push-pull systems, as confirmed by studies including steady-state and time-resolved fluorescence, and femtosecond transient absorption studies.

EXPERIMENTAL SECTION

General Methods

All the moisture and oxygen-sensitive reactions were performed in an inert atmosphere using the standard inert atmosphere method .^{1}H NMR was measured in Bruker Avance (III) 500 MHz, and ^{13}C NMR spectra were measured in 126 MHz using $CDCl_3$ as the internal solvent. The ^{1}H NMR chemical shifts are recorded in parts per million (ppm) relative to the solvent residual peak ($CDCl_3$, 7.26 ppm). The ^{13}C NMR shifts are reported relative to the solvent residual peak ($CDCl_3$, 77.00 ppm). The multiplicities are given as s (singlet), d (doublet), t (triplet), q (quartet), m (multiplet),

and the coupling constants values (*J*) are reported in Hz. The UV-visible absorption spectra of all compounds were recorded in PerkinElmer's LAMBDA 35 UV-visible Spectrophotometer in DCM solvent at room temperature. High-Resolution Mass Spectrometry (HRMS) was recorded on a Bruker-Daltonics micrOTOF-Q II mass spectrometer. The cyclic voltammogram and differential voltammogram (DPVs) were recorded on electrochemical analyzer using glassy carbon as the working electrode, Pt wire as the counter electrode and the Ag/AgCl as the reference electrode. Thermogravimetric analysis was performed on the Mettler Toledo thermal analysis system.

Synthesis and characterization of BODIPY 1: Under argon atmosphere, a solution of compound **1** (8-chloro BODIPY) (0.1 g, 0.44 mmol) and the corresponding compound **2** (0.064 g, 0.44 mmol) in dry THF (20 ml), added triethylamine (TEA) (20 ml), $Pd(PPh_3)_4$ (0.016 g, 0.022 mmol), CuI (0.004 g, 0.022 mmol), stirred for 2 h at 0 °C, after completion of the reaction, the reaction mixture was concentrated under reduced pressure, the crude compound was purified by column chromatography on silica, using Hexane/ DCM (70:30, v/v), and afforded pure **BODIPY 1** (Purple color) around 80 % yield. ^{1}H NMR (500 MHz, $CDCl_3$) δ 7.76 (s, 2H), 7.54 (d, *J* = 8.9 Hz, 2H), 7.37 (d, *J* = 3.9 Hz, 2H), 6.69 (d, *J* = 8.9 Hz, 2H), 6.52 (d, *J* = 2.9 Hz, 2H), 3.09 (s, 6H); ^{13}C NMR (126 MHz, $CDCl_3$) δ 152.21, 141.61, 136.03, 135.21, 129.16, 127.85, 117.59, 112.68, 111.88, 106.92, 86.68, 40.20; HRMS (ESI, positive) m/z calculated for $C_{19}H_{16}BF_2N_3$ 358.1301 $[M + Na]^+$, measured 358.1306 $[M + Na]^+$.

Synthesis and characterization of BODIPY 2: Under argon atmosphere, a solution of compound **1** (8-chloro BODIPY) (0.1 g, 0.44 mmol) and the corresponding compound **3** (8-chloro BODIPY) (0.108 g, 0.44 mmol) in dry THF (20 ml), added triethylamine (TEA) (20 ml), $Pd(PPh_3)_4$ (0.016 g, 0.022 mmol), CuI (0.004 g, 0.022 mmol), stirred for 2 h at 0 °C, after completion of the reaction, the reaction mixture was concentrated under reduced pressure, the crude compound was purified by column chromatography on silica, using Hexane/ DCM (60:40, v/v), and afforded pure **BODIPY 2** (Brown color) around 70 % yield. ^{1}H NMR (500 MHz, $CDCl_3$) δ 7.83 (s, 2H), 7.62 (d, *J* = 8.3 Hz, 2H), 7.55 (d, *J* = 8.3 Hz, 2H), 7.42 (dd, *J* = 12.9, 6.4 Hz, 4H), 6.67 (d, *J* = 8.8 Hz, 2H), 6.56 (d, *J* = 3.6 Hz, 2H), 3.02 (s, 6H); ^{13}C NMR (126 MHz, $CDCl_3$) δ 150.64, 143.71, 133.17, 132.81, 131.59, 129.16, 127.53, 119.39, 118.51, 111.91, 109.19, 106.13, 95.58, 87.44, 85.80,

40.30; HRMS (ESI, positive) m/z calculated for $C_{27}H_{20}BF_2N_3$ 436.1796 $[M + H]^+$, measured 436.1836 $[M + H]^+$.

Synthesis and characterization of BODIPY 3: In a 50 mL round-bottomed flask, tetracyanoethylene (TCNE, 32 mg, 0.25 mmol) was added to the solution of BODIPY **2** (100 mg, 0.22 mmol) in DCM (20 mL). The reaction mixture was stirred at room temperature for 6 h. After completion of the reaction, the reaction mix. was dried under vacuum and purified by column chromatography with Hexane/DCM (30:70, v/v) as eluent to give BODIPY **3** as a dark red solid (Yield: 75 %). ^{1}H NMR (500 MHz, $CDCl_3$) δ 7.86 (s, 2H), 7.82 – 7.77 (m, 6H), 7.36 (d, *J* = 4.1 Hz, 2H), 6.77 (d, *J* = 9.4 Hz, 2H), 6.58 (d, *J* = 3.9 Hz, 2H), 3.20 (s, 6H); ^{13}C NMR (126 MHz, $CDCl_3$) δ 167.94, 162.50, 154.73, 144.91, 133.57, 132.67, 129.90, 129.57, 126.73, 119.11, 118.00, 112.59, 111.85, 101.76, 88.86, 87.48, 40.40; HRMS (ESI, positive) m/z calculated for $C_{33}H_{20}BF_2N_7$ 564.1920 $[M + H]^+$, measured 564.1940 $[M + H]^+$.

Synthesis and characterization of BODIPY 4: In 50 mL round-bottomed flask, tetracyanoquinodimethane (TCNQ, 51 mg, 0.25 mmol) was added to a solution of BODIPY **2** (100 mg, 0.22 mmol) in DCE (20 mL) under argon atmosphere. The reaction mixture was heated at 60 °C for 8 h. After completion of the reaction, the reaction mixture was dried under vacuum and purified by column chromatography with hexane/DCM (20:80, v/v) (eluent: CH_2Cl_2) BODIPY **4** as dark black (Yield: 71%). ^{1}H NMR (500 MHz, $CDCl_3$) δ 7.86 (s, 2H), 7.72 (s, 4H), 7.48 (dd, *J* = 9.6, 1.8 Hz, 1H), 7.33 (d, *J* = 4.0 Hz, 2H), 7.30 (dd, *J* = 9.6, 1.8 Hz, 1H), 7.27 (s, 1H), 7.25 (s, 1H), 7.20 (dd, *J* = 9.5, 1.8 Hz, 1H), 6.97 (dd, *J* = 9.6, 1.8 Hz, 1H), 6.73 (d, *J* = 9.1 Hz, 2H), 6.56 (d, *J* = 3.7 Hz, 2H), 3.14 (s, 6H); ^{13}C NMR (126 MHz, $CDCl_3$) δ 171.21, 153.98, 153.07, 150.77, 144.83, 136.68, 135.82, 134.57, 134.11, 133.52, 132.44, 130.00, 129.47, 125.85, 125.46, 123.53, 119.03, 114.70, 112.72, 102.05, 89.03, 87.18, 72.83, 40.32. HRMS (ESI, positive) m/z $[M + Na]^+$ calculated for $C_{39}H_{24}BF_2N_7$ 662.2053, measured 662.2063 $[M+ Na]^+$.

RESULTS AND DISCUSSION

The **BODIPYs 1** and **2** and control compound **C1** were synthesized by the palladium-catalyzed Sonogashira cross-coupling reaction in good yields. The push-pull **BODIPYs 3** and **4**

were synthesized by the [2+2] cycloaddition-retroelectrocyclization (CA-RE) reaction of **BODIPY 2** with strong acceptor TCNE and TCNQ units. The control compound **C1** and precursor 8-chloro BODIPY were synthesized by the reported procedure in good yield.[22] The **BODIPY 1** was synthesized by the reaction of 8-chloro **BODIPY** with 4-ethynyl-*N,N*-dimethylaniline using catalytic amount of $Pd(PPh_3)_2Cl_2$ in tetrahydrofuran (THF) and triethylamine (TEA) solvent at 0 °C for 2 hours, in 80% yield. Similarly, **BODIPY 2** was synthesized *via* reaction of 8-chloro **BODIPY** with 4-((4-ethynylphenyl)ethynyl)-*N, N*-dimethylaniline using a catalytic amount of Pd $(PPh_3)_2Cl_2$ in tetrahydrofuran (THF) and triethylamine (TEA) solvent at 0 °C for 2 hours, in 70% yield (Scheme 1).

The push-pull **BODIPY 3** was synthesized by the reaction of **BODIPY 2** with TCNE at room temperature for 6 h in dichloromethane (DCM) which resulted in 75% yield. Similarly, the **BODIPY 4** was synthesized by the reaction of **BODIPY 2** with TCNQ in DCE solvent at reflux conditions for 8 h which resulted in 71% yield (Scheme 1).

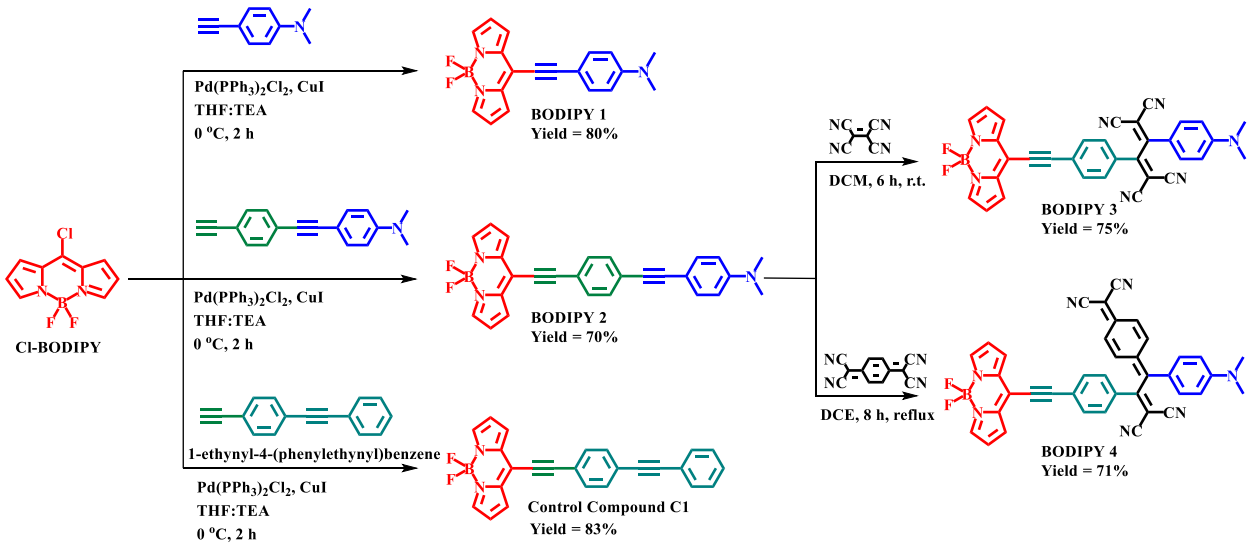

Scheme 1. Synthetic methodology of push-pull **BODIPYs 1–4** and control compound **C1**.

The push-pull **BODIPYs 1–4** and control compound **C1** were purified by silica-gel column chromatography (silica gel size = 100–200 mesh) using Hexane: DCM as a solvent. The **BODIPYs 1–4** exhibit good solubility in common organic solvent acetone, chloroform, dichloromethane, and acetonitrile. The ^{1}H NMR, ^{13}C NMR, and HRMS techniques were used to characterize the

molecular structures of the push-pull BODIPYs. (see Figures S1-S12 in the supporting information).

Photophysical properties

The electronic absorption spectra of the studied control compound **C1** and push-pull **BODIPYs 1–4** were carried out in three distinct polarity solvents: benzonitrile (light blue), dichlorobenzene (red), and toluene (brown) at room temperature as shown in Figure 1 and the data are summarized in Table 1.

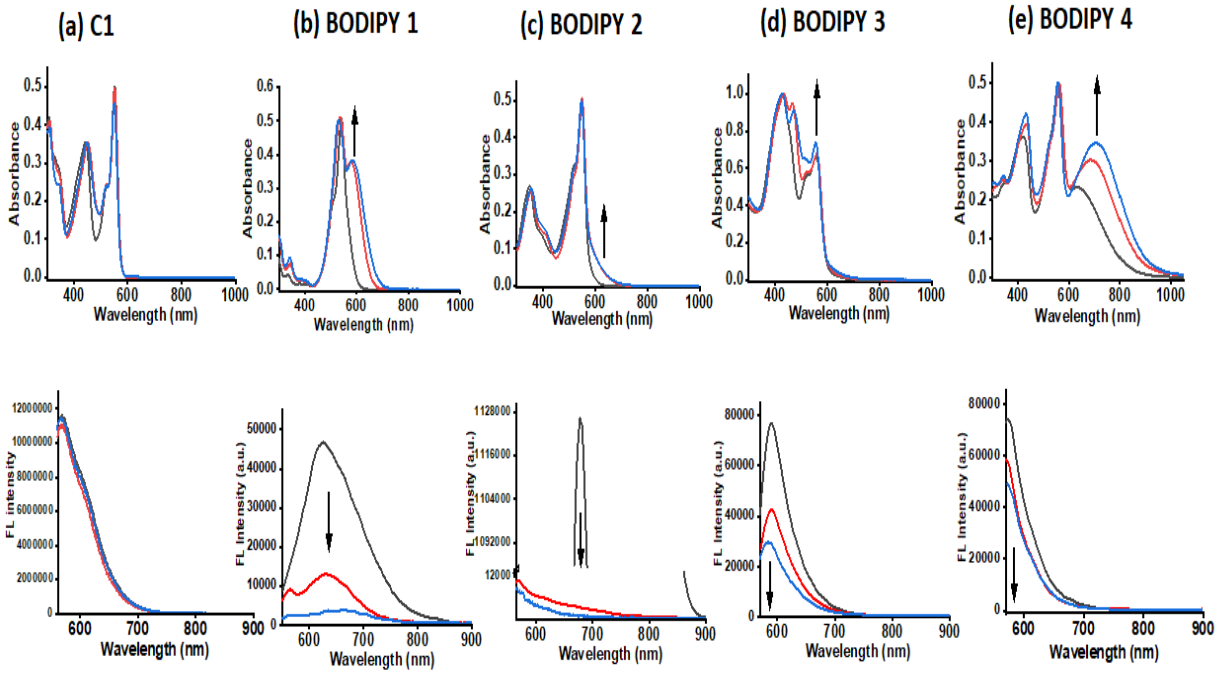

Figure 1. Normalized to the BODIPY visible band, absorption spectra of (a) **C1**, (b) **BODIPY 1**, (c) **BODIPY 2**, (d) **BODIPY 3**, and (e) **BODIPY 4** along with fluorescence spectra which the lower panel in solvents of varying polarity ((benzonitrile (light blue), dichlorobenzene (red), and toluene (brown)). Samples were excited at the peak near 550 nm.

In general, simple pristine BODIPY exhibits an absorption band around 500 nm.[12-14] The NND-BODIPYs exhibited an intense absorption band at the 450–550 nm region due to the $S_0 \rightarrow S_1$ ($\pi \rightarrow \pi^*$) transition. The control compound **C1** shows absorption at 311 nm, 445 nm, 517 nm (sh), and 553 nm. The **BODIPYs 1** and **2** shows the absorption at 344 nm, 538 nm, 581 nm and 357 nm, 517 nm (sh), 550 nm, respectively, and these electronic absorption bands correspond to π–π^*

transitions. The **BODIPYs 3** and **4** exhibit absorption at 435 nm, 470 nm, 561 nm and 338 nm, 431 nm, 561 nm, 689 nm, respectively.

Table 1. Photophysical and electrochemical data of push-pull BODIPYs 1–4 and C1.

	Photophysical data[a]			Electrochemical data[b]			τ_{av} (ns)[c]
Compound	λ_{abs} **(nm)**	λ_{em} **(nm)**	**Optical band gap (eV)**	E_{ox} **(V)**	E_{red} **(V)**	$\Delta E_{1/2}$	
C1	311, 452, 517 (sh), 552	568	2.16	1.79	-0.48 -1.26	2.27	2.65
BODIPY 1	344, 538 581	630	1.83	1.09	-0.57 -1.46	1.66	0.43
BODIPY 2	357, 517 (sh) 550	567	1.66	0.95 1.68	-0.43 -1.23	1.38	1.29
BODIPY 3	435, 470 561	590	2.01	1.40	-0.26 -0.37 -0.76 -1.48	1.66	--
BODIPY 4	338, 431, 561 689	570	1.18	0.94	-0.08 -0.21 -0.47 -1.40	1.02	--

[a]Absorbance recorded in DCB at 1×10^{-5} M conc. λ_{abs}: absorption wavelength. λ_{em}: emission wavelength. [b] Electrochemical analysis was estimated by differential pulse voltammetry in 0.1 M solution of Bu_4NPF_6 in DCB at 100 mV s^{-1} scan rate *versus* Ag/AgCl at 25 °C. E_{oxi} and E_{red} values are based on DPV analysis. [c] Emission decay lifetime in DCB after exciting at the peak near 550 nm.

The absorption bands at the shorter wavelength region corresponds to π–π* transitions from NND unit, and at the higher wavelength region were associated to π–π* transitions from BODIPY unit. The push-pull **BODIPYs 3,** and **4** display a bathochromic shift compared to **BODIPY 1** and **2** due to significant donor-acceptor interaction. Different polarity solvents were used in this study to examine the impact of polarity on absorbance. It was found, surprisingly, that for newly synthesized donor-acceptor systems **BODIPYs 1-4**, increasing the polarity of the solvent led to

the emergence of a new peak at the higher wavelength region, with an increasing intensity (represented by an arrow in Figure 1). However, this trend was not seen for the control compound **C1**.

The optical bandgap calculated from the onset wavelength of the UV-Visible spectrum of the push-pull **BODIPYs 1–4** follows the order **3** >**1** > **2**> **4** which indicates that the introduction of strong acceptor results in low optical band gap with a red-shifted ICT band in electronic absorption spectra. The DCNQ substituted **BODIPY 4** exhibit a red shifted ICT band at longer wavelength region compared to TCBD substituted **BODIPY 3** due to strong electronic communication between donor and acceptor unit.

Fluorescence emission was also recorded for the control compound **C1** and **BODIPYs 1–4** to evaluate the effect of TCBD and DCNQ. Among all studied compounds, **C1** was found to be the highly fluorescent, and its peak intensities were nearly unaffected by the solvent's polarity. The fluorescence intensity was significantly reduced for **BODIPYs 1–4** and it was noticed that the polarity of the solvents had a significant impact on the peak's intensity for all push-pull systems as illustrated in Figure 1. Based on the observed results while recording absorbance and fluorescence, the peak shown by an arrow in absorption spectra could be assigned to intramolecular charge transfer (ICT) band due to strong interactions between donor and acceptor moieties which was not seen in control compound **C1**.[47] Quenching of the emission for **BODIPYs 1–4** suggest that excited state processes are taking place in newly synthesized push-pull systems. Next, the fluorescence lifetime was measured for these compounds in distinct polarity solvents using the time-correlated single-photon counting (TSCPC) method using a nanoLED excitation source as shown in Figure S13, and the obtained data are summarized in Table 1.

Electrochemical properties

The electrochemical properties of the push-pull **BODIPYs 1–4** were explored by using cyclic voltammetry (CV) and differential pulse voltammetry (DPV) techniques. All the measurements were recorded in dichlorobenzene solvent at room temperature using (TBA)ClO_4 as a supporting electrolyte. The representative differential pulse voltammograms (DPVs) of control compound **C1** and **BODIPYs 1–4** are shown in Figure 2, and the data of push-pull **BODIPYs 1–4** are summarized in Table 1. The cyclic voltammograms (CVs) plots of **C1** and **BODIPYs 1–4** are shown in Figure S14 (Supporting Information).

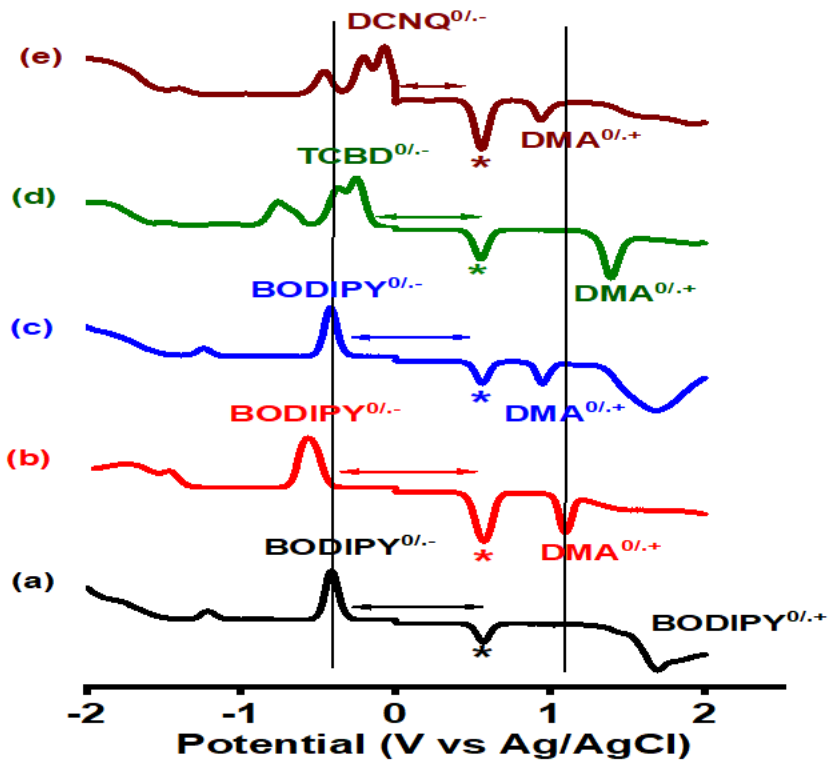

Figure 2. Differential pulse voltammograms of (a) **C1**, (b) **BODIPY 1**, (c) **BODIPY 2**, (d) **BODIPY 3**, and (e) **BODIPY 4** in dichlorobenzene containing 0.1 mol/L (TBA)ClO_4 supporting electrolyte at 298K. The '*' indicates ferrocene oxidation used as an internal standard.

The redox-active moieties exhibit an individual oxidation and reduction potential which are crucial in determining their ability in the electron transfer system. The donor NND unit exhibited a reversible single oxidation at low potential. The BODIPY generally shows single oxidation due to the formation of a mono π-radical cation and two reductions due to the formation of mono and di anion species.[51] The control compound **C1** exhibited one oxidation at 1.69 V and two reductions at –0.42 and –1.21 V vs Ag/AgCl. **BODIPY 1** exhibited one oxidation process at 1.09 V and two reduction processes at –0.57 and –1.46 V. **BODIPY 2** showed two oxidation processes at 0.95 and 1.7 V, the first is attributed to the formation of mono radical cation $NND^{\cdot+}$ and second oxidation is attributed to $BODIPY^{\cdot+}$. The same molecule exhibited two reductions at –0.43 and –1.23 V, both are attributed to the formation of $BODIPY^{\cdot-}$ and $BODIPY^{-2}$.

The push–pull **BODIPYs 3** and **4** exhibited first oxidation due to the formation of $NND^{\cdot+}$ and four reduction processes in the applied potential window. The initial first two reductions were

observed due to the formation of mono and di-anion formation of the TCBD unit and each step corresponds to a one electron transfer and last two reductions were observed due to the formation of the BODIPY mono and di-anions.[34] The comparison of **BODIPYs 3** and **4** indicates that **BODIPY 4** is easier to reduce than **BODIPY 3**, which can be attributed to the better electron acceptor nature of DCNQ.[40]

Thermal Properties

The thermal properties of the push–pull **BODIPYs 1–4** were measured by thermogravimetric analysis (TGA) at a heating rate of 10 ºC min^{-1} and monitoring the weight loss against temperature under the nitrogen atmosphere.

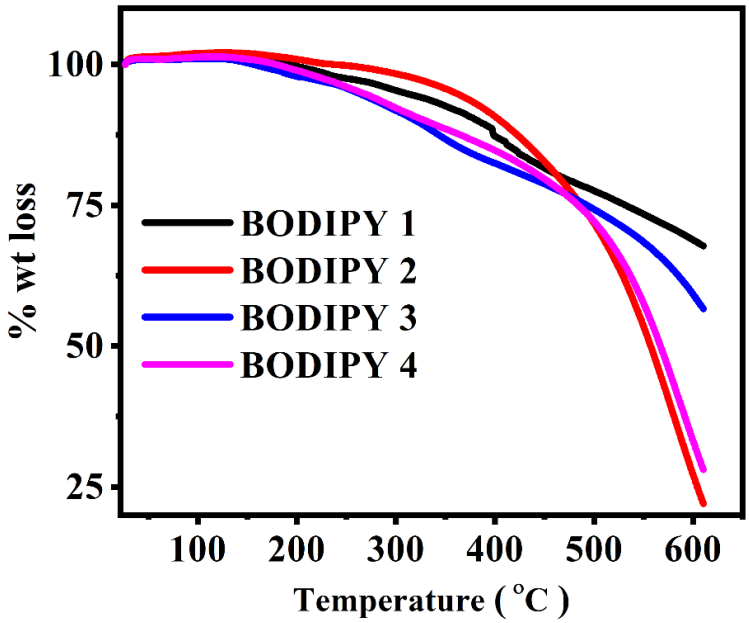

Figure 3. Thermogravimetric analysis (TGA) of the push–pull **BODIPYs 1–4** measured at a heating rate of 10 ℃ min^{-1} under a nitrogen atmosphere.

The push–pull **BODIPYs 1–4** exhibit excellent thermal stability and the corresponding thermograms are shown in Figure 3. The decomposition temperatures for the **BODIPYs 1–4** at 5% weight loss were found to be 315 ℃, 364 ℃, 261 ℃, and 275 ℃, respectively. The *N,N*-dimethylaniline functionalized **BODIPY 2** exhibits the highest thermal stability as compared to **BODIPYs 1, 3,** and **4**. The DCNQ-functionalized **BODIPY 4** exhibits higher thermal stability

than TCBD-functionalized **BODIPY 3**. The thermal stability of the push–pull **BODIPYs 1–4** follows the order **2**> **1**> **4**> **3**.

Theoretical calculations

The density functional theory (DFT) calculations were performed to understand the geometry and electronic properties of the push-pull **BODIPYs 1–4** at the B3LYP/6-31G (d, p) level for C, H, N, B, and F using *Gaussian 09W* program. The optimized structures of the push-pull **BODIPYs 3** and **4** exhibit twisted geometry due to the incorporation of strong acceptor TCBD and DCNQ (Table S1). The push-pull **BODIPYs 1–4** show that the HOMOs are localized over donor NND and BODIPY unit, whereas the LUMOs are localized on strong acceptor, TCBD, DCNQ, and BODIPY unit. In the case of **BODIPY 4**, the HOMOs are localized on the donor NND unit and LUMOs are mostly centered on the strong acceptor DCNQ unit which indicates a strong charge transfer from the donor to the acceptor unit. The energy level diagram and frontier molecular orbitals of **BODIPYs 1–4** are shown in Figure 4.

The push-pull **BODIPY 4** exhibits the lowest HOMO–LUMO gap and signifies that the DCNQ unit acts as a strong acceptor compared to the TCBD unit. The theoretically predicted HOMO energy levels of the push-pull **BODIPYs 1–4** are –5.53 eV, –5.21 eV, –6.06 eV, and –5.73 eV, and associated LUMO levels are –2.73 eV, –2.95 eV, –3.65 eV and –3.91 eV, respectively. The introduction of TCBD and DCNQ unit stabilized the LUMO energy levels, which resulted in a red shifted ICT band in electronic absorption spectra. (Figure 4). The trend in the LUMO energy level of **BODIPYs 3** and **4** follows the order **3** > **4**, which suggests that decreasing the LUMO energy levels will increase the strength of the acceptor unit. The computationally calculated HOMO–LUMO gap values of the push-pull **BODIPYs 1–4** are 2.80, 2.26, 2.41, and 1.82 eV, respectively. The electronic transitions with oscillator strengths, composition, and assignment data are tabulated in Table S2 (SI). The optical bandgap (E_{gap}) values calculated from UV-visible spectra agreed well with the theoretically predicted HOMO–LUMO gap trends.

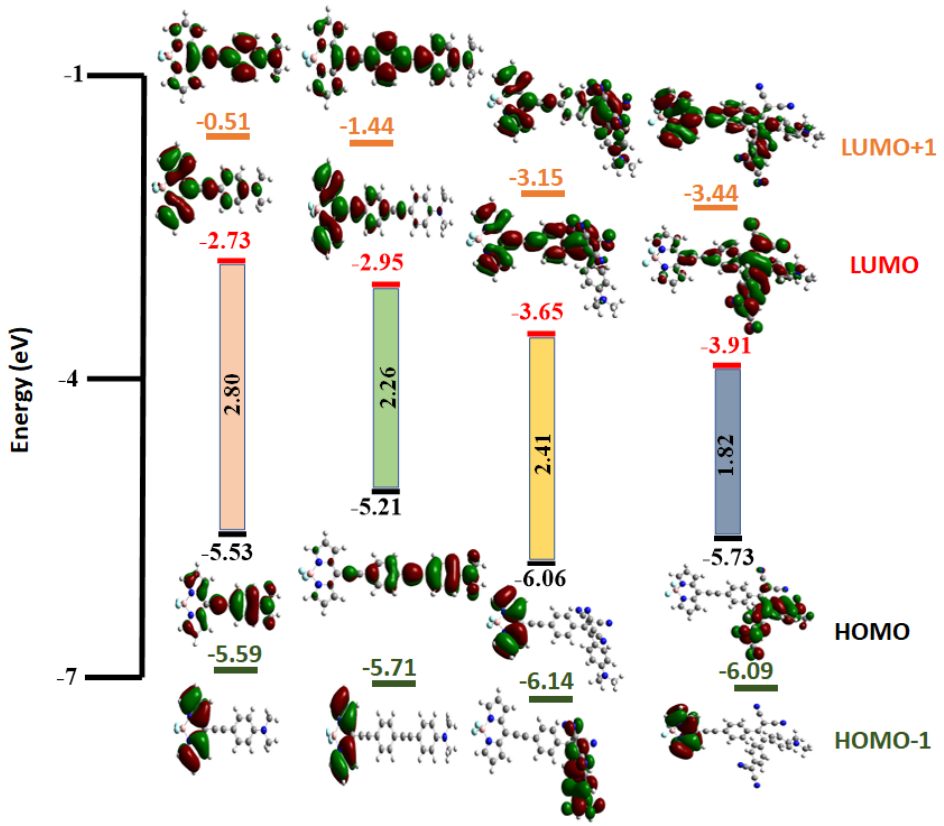

Figure 4. Energy level diagram and frontier HOMO–1, HOMO, LUMO and LUMO+1 orbitals of push-pull **BODIPYs 1–4** estimated by DFT calculations (B3LYP/631G (d, p) level).

The time-dependent DFT (TD-DFT) calculations were also performed to evaluate the electronic transitions of the push–pull **BODIPYs 1–3** at B3LYP/6-31G (d, p) and CAM-B3LYP/6-31G (d, p) level for the **BODIPY 4**, in DCM solvent. The polarized continuum model (PCM) was used to analyse the solvent effect in TD-DFT calculation. The TD-DFT data of the push–pull **BODIPYs 1–4** are compiled in Table S2 (SI). The **BODIPYs 1** and **2** exhibit absorption bands at 441 nm, 542 nm and 456 nm, 693 nm, respectively (S16). The absorption band at higher wavelength region originates from HOMO → LUMO, and at the lower wavelength region occurs from HOMO–1 → LUMO, attributed to π–π* transition for **BODIPYs 1** and **2**. The TCBD and DCNQ substituted **BODIPYs 3** and **4** exhibit two absorption bands: at a shorter wavelength region attributed to the π–π* transition and ICT at a longer wavelength region. The **BODIPYs 3** and **4** exhibit absorption bands at 447 nm, 505 nm and 452 nm, 629 nm, respectively (S16). The absorption band at the lower wavelength region for **BODIPYs 3** and **4** originates from HOMO–2 → LUMO and HOMO–1 to LUMO+1 attributed to π–π* transition. The **BODIPYs 3** and **4** exhibit

the ICT band at longer wavelength region originating from HOMO → LUMO+1 and HOMO → LUMO transition.

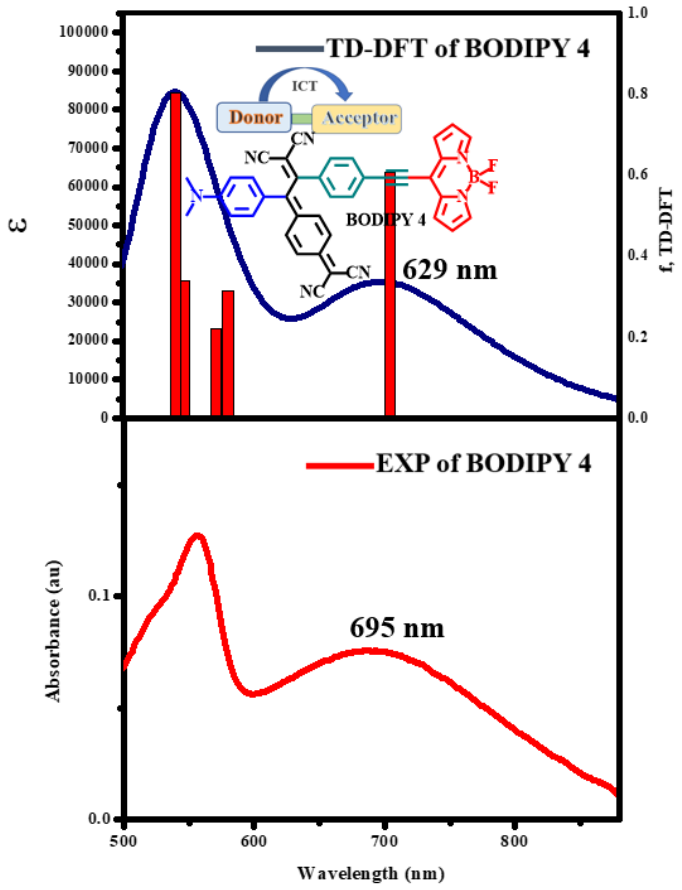

Figure 5. UV-vis absorption spectra of push–pull **BODIPY 4**. Experimental (bottom) and TD-DFT predicted (top) in DCM solvent.

The theoretically calculated electronic absorption wavelengths (Figure 5) were found to be longer than experimental data, which could be due to several factors such as solvent effect, temperature, and dipole moment.

Free-energy calculations and energy level diagram

From the spectral, computational calculations, and electrochemical data, Jablonski-type energy level diagrams were constructed to predict different possible photochemical processes in newly synthesized donor-acceptor systems (Figure 6). The HOMO-LUMO gap in the gaseous phase from the computational studies was used for the charge transfer (CT) state in case of

BODIPY 4, in energy profile diagram. The change in Gibbs free-energy for charge separation and recombination was obtained by using equations i–iii:

$-\Delta G_{CR} = E_{ox} - E_{red} + \Delta Gs$ (i)

$-\Delta G_{CS} = \Delta E_{00} - (-\Delta G_{CR})$ (ii)

where ΔE_{00} corresponds to the singly excited state energy for the control compound, **C1**. The term ΔGs refers to electrostatic energy calculated according to the dielectric continuum model (see eq iii). The E_{ox} and E_{red} stand for the first oxidation and reduction potential of push-pull systems, respectively.

$$\Delta G_S = \frac{e^2}{4\Pi\varepsilon_0}\left[\left(\frac{1}{2R_+} + \frac{1}{2R-}\right)\Delta\left(\frac{1}{\varepsilon_R}\right) - \frac{1}{R_{cc}\varepsilon_R}\right] \quad \text{(iii)}$$

The symbols ε_0 and ε_R indicates the permittivity of vacuum and dielectric constant of dichlorobenzene used for photochemical and electrochemical experiments (= 9.93). The symbols R_+ and R_- represent the radii of the cation and anion, respectively R_{cc} represents the center-to-center distance between donor and acceptor parts of the synthesized dyad and triad from the computed structures as shown in Figure 4.

For the compounds, **C1** and **BODIPYs 1–4**, selective excitation of BODIPY entities corresponding to its π–π* (locally excited LE) transitions would lead to populate the singlet excited state of BODIPY resulting in the formation of ^{1}BODIPY*. According to the constructed energy profile diagram in Figure 6, the following processes were observed upon excitation: (i) In the case of **BODIPYs 1–2**, due to facile oxidation of NND over BODIPY, the singlet excited state of BODIPY (^{1}BODIPY*) would lead to populating the thermodynamically feasible charge-separated state BODIPY$^{\cdot-}$-NND$^{\cdot+}$, and BODIPY$^{\cdot-}$-Ph-NND$^{\cdot+}$ for **BODIPY 1** and **BODIPY 2**, respectively. iii) as anticipated, oxidation of NND was shown to be easier than BODIPY in the case of BODIPYs **3-4** and the incorporation of TCBD and DCNQ makes these compounds considerably easier to reduce which preferred the formation of (BODIPY-Ph-TCBD)$^{\cdot-}$-NND$^{\cdot+}$ and (BODIPY-Ph-DCNQ)$^{\cdot-}$-NND$^{\cdot+}$ for **BODIPY 3** and **BODIPY 4**, respectively. Electrochemistry results indicate that electrons are being transferred from donor NND to acceptor (TCBD and DCNQ) and after comparing this result with the DFT calculations, we can conclude that HOMO → LUMO+1 transition is the appropriate transition that favors the expected directionality of charge and electron

transfer in **BODIPY 3**. The energy gap for this transition from the computed structure was found to be 2.4 eV for **BODIPY 3.** Since this gap (2.4 eV) for **BODIPY 3** is significantly higher than the singlet excited state, it is likely that ^{1}BODIPY* would directly lead to populating the thermodynamically feasible charge separated state (BODIPY-Ph-TCBD)$^{\cdot-}$-NND$^{\cdot+}$ without the formation of CT state (BODIPY-Ph-TCBD)$^{\delta-}$-NND$^{\delta+}$, which cannot be accessed. Whereas for **BODIPY 4**, the HOMO-LUMO gap from the computed structure was found to be 1.82 eV which favored the formation of (BODIPY-Ph-DCNQ)$^{\delta-}$-NND$^{\delta+}$ followed by charge-separated state (BODIPY-Ph-DCNQ)$^{\cdot-}$-NND$^{\cdot+}$ in case of **BODIPY 4.**

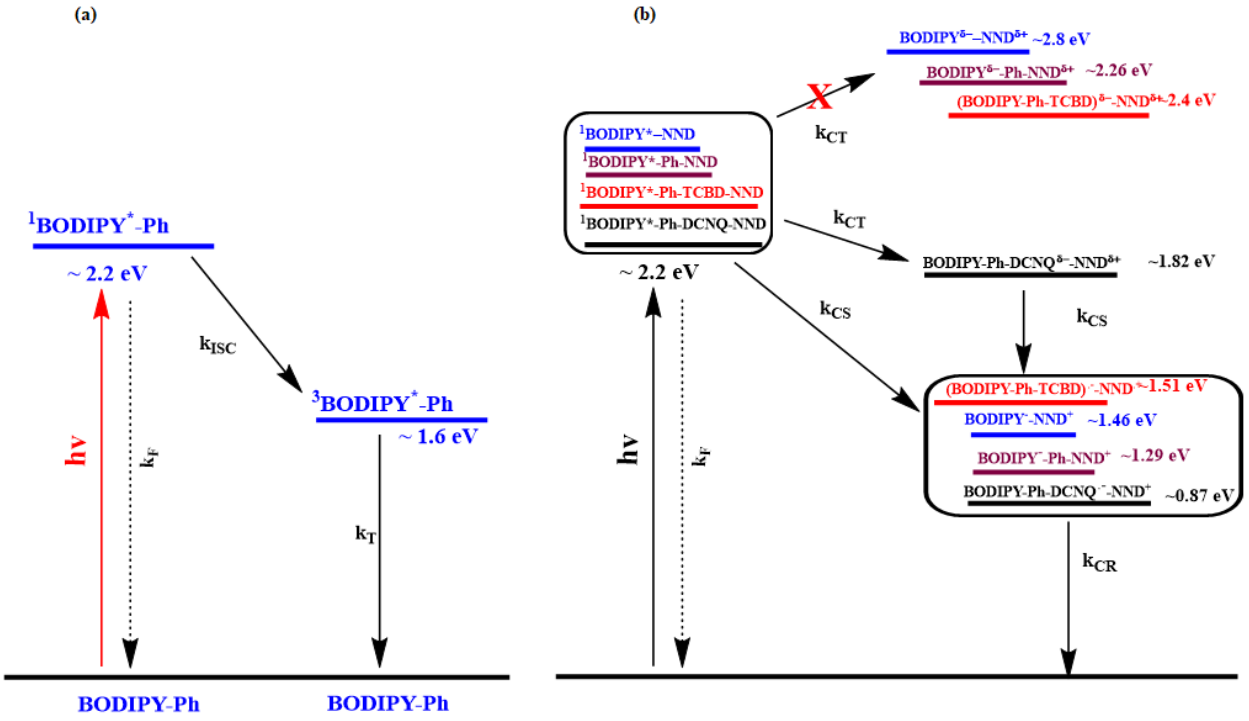

Figure 6. Jablonski type energy level diagram for the (a) control BDP-Ph and (b) indicated push-pull systems in dichlorobenzene. Abbreviations: CS = charge separation, CT = charge transfer, CR = charge recombination, ISC = intersystem crossing, F = fluorescence emission, T = triplet emission. E_{CT} are gas phase HOMO-LUMO gap.

Next, spectroelectrochemical studies were carried out on this series of push-pull systems, to describe the expected electron transfer product, originating upon photoexcitation during transient absorption studies. These spectra were acquired by applying the appropriate potential, 100 mV past the first oxidation and first reduction potential for each compound. During the first oxidation of control compound **C1**, decreasing the intensity of original peaks resulted in the

development of a broad new peak from 590–1300 nm, and one isosbestic point was also observed at 575 nm. Whereas, during the first reduction process, decreasing the intensity of original peaks resulted in the development of new peaks at 375 nm, and 580 nm, and three isosbestic points were observed at 312 nm, 721 nm, and 900 nm. In the case of **BODIPY 1**, during the first oxidation, decreasing the intensity of original peaks resulted in the formation of new peaks at 389 nm and a broad new peak from 682–1300 nm, and two isosbestic points were also observed at 472 nm, and 668 nm. Whereas, during the first reduction process, decreasing the intensity of original peaks resulted in the formation of new peaks at 394 nm, 553 nm, and a weak broad peak from 755–1000 nm, and two isosbestic points were observed at 394 nm, and 553 nm. For **BODIPY 3**, during the

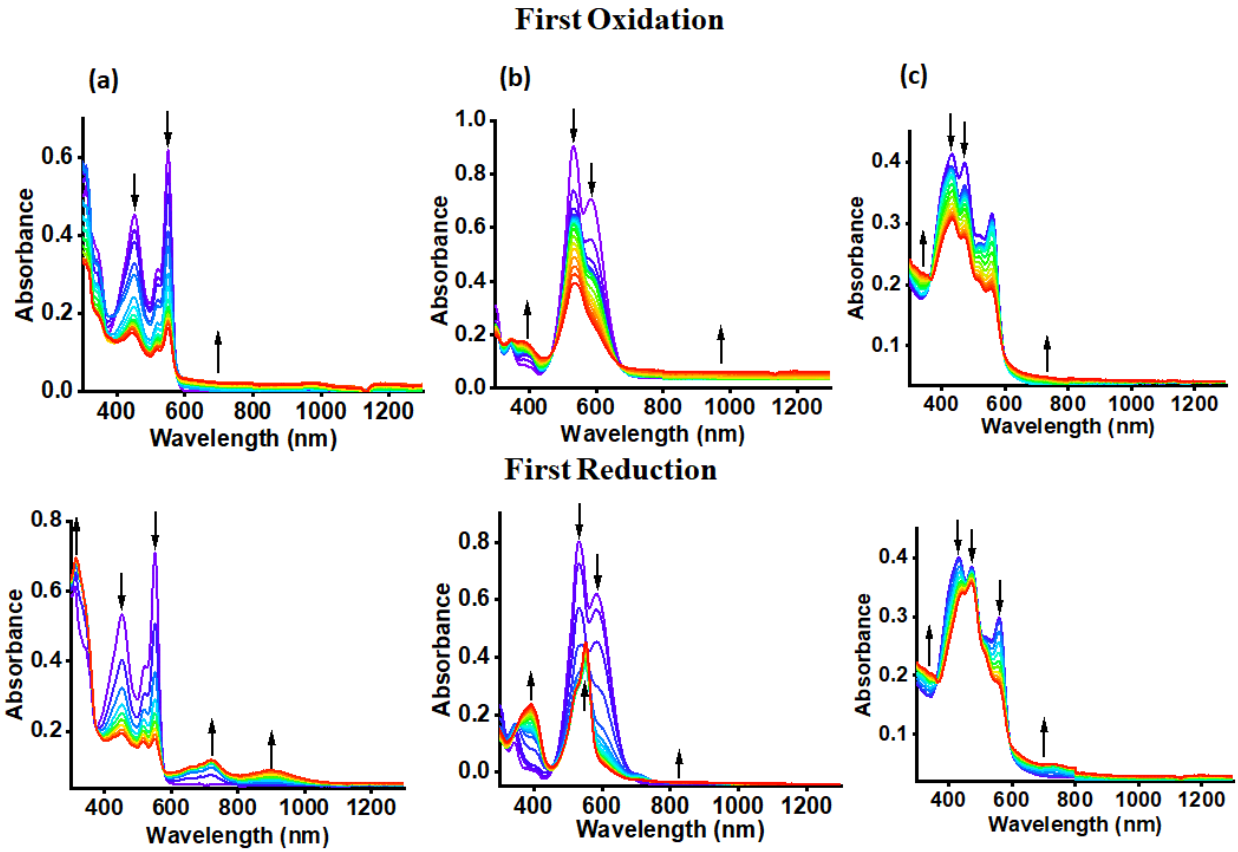

Figure 7. Spectral changes during the first oxidation (top) and first reduction (bottom) of (a) **C1**, (b) **BODIPY 1**, and (c) **BODIPY 3**.

first oxidation, decreasing the intensity of original peaks resulted in the generation of a new broad peak at 615–1300 nm, and two isosbestic points were also observed at 366 nm, and 600 nm.

Whereas, during the first reduction process, decreasing the intensity of original peaks resulted in the generation of new peaks at 335 nm, and a broad peak from 598–1300 nm and two isosbestic points were observed at 367 nm, and 593 nm as shown in Figure 7. Almost similar kind of spectral features were observed for remaining two push-pull systems **BODIPY 2**, and **BODIPY 4** as shown in Figure S15.

Femtosecond-transient-absorption studies

Femtosecond transient spectra of push-pull series were recorded in dichlorobenzene, by exciting BODIPY entities, corresponding to the locally excited state. Figure 8a shows the transient spectra along with species-associated spectra (SAS) for the control compound **C1** at indicated delay times. The instant formation of ^{1}BODIPY* exhibited one strong excited state absorption band at 487 nm. The slower decaying of this peak could be ascribed to ^{3}BODIPY* before returning to the ground state. In addition, one broad negative peak was observed at 550 nm. By comparison with absorption and fluorescence, this peak was associated to the ground state bleaching (GSB) overlapped with stimulated emission (SE). Further, the data was analyzed by GloTarAn analysis by fitting $S_0 \rightarrow S_1 \rightarrow T_1 \rightarrow GS$ model as shown in Figure 8b. The lifetimes were found to be 2 ps for S_1^{*}, 1.6 ns for S_1 and >3 ns for T_1.

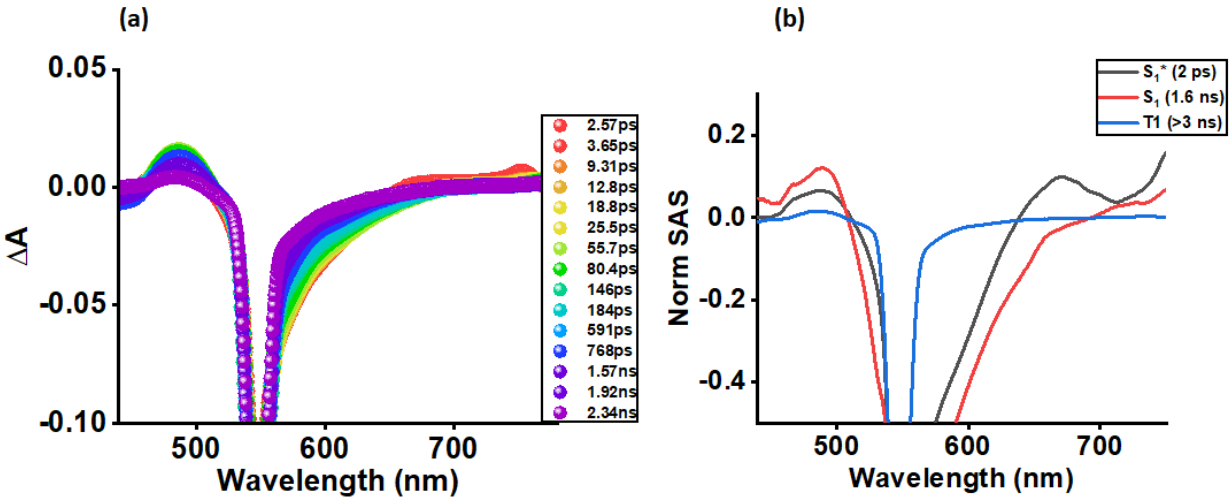

Figure 8. (a) Fs-TA spectra of **C1** at the indicated delay times in dichlorobenzene at the excitation wavelength of 551 nm. (b) Species-associated spectra from GloTarAn analysis. The data was fitted to a three-component fit representing S_1^{*}, S_1, and T_1 states.

Figure 9 shows the femtosecond transient absorption spectra for **BODIPYs 1–2** at the indicated delay times in dichlorobenzene. For **BODIPY 1** (Figure 9a), excited state absorption (ESA) peaks were observed at 460 and 650 nm corresponding to both S_1 and CS states. Within 2 ps, the formation of ^{1}BODIPY* took place at 460 nm, and in the next 20–30 ps, a new broad peak started emerging at 650 nm which could be assigned to the charge-separated state. Complete decaying of this peak in a given time delay time shows that CS is directly relaxing back to the ground state without populating a long-lived triplet state. Furthermore, one broad negative peak was detected at 532 nm corresponding to GSB. Figure 9b shows the SAS for **BODIPY 1** after

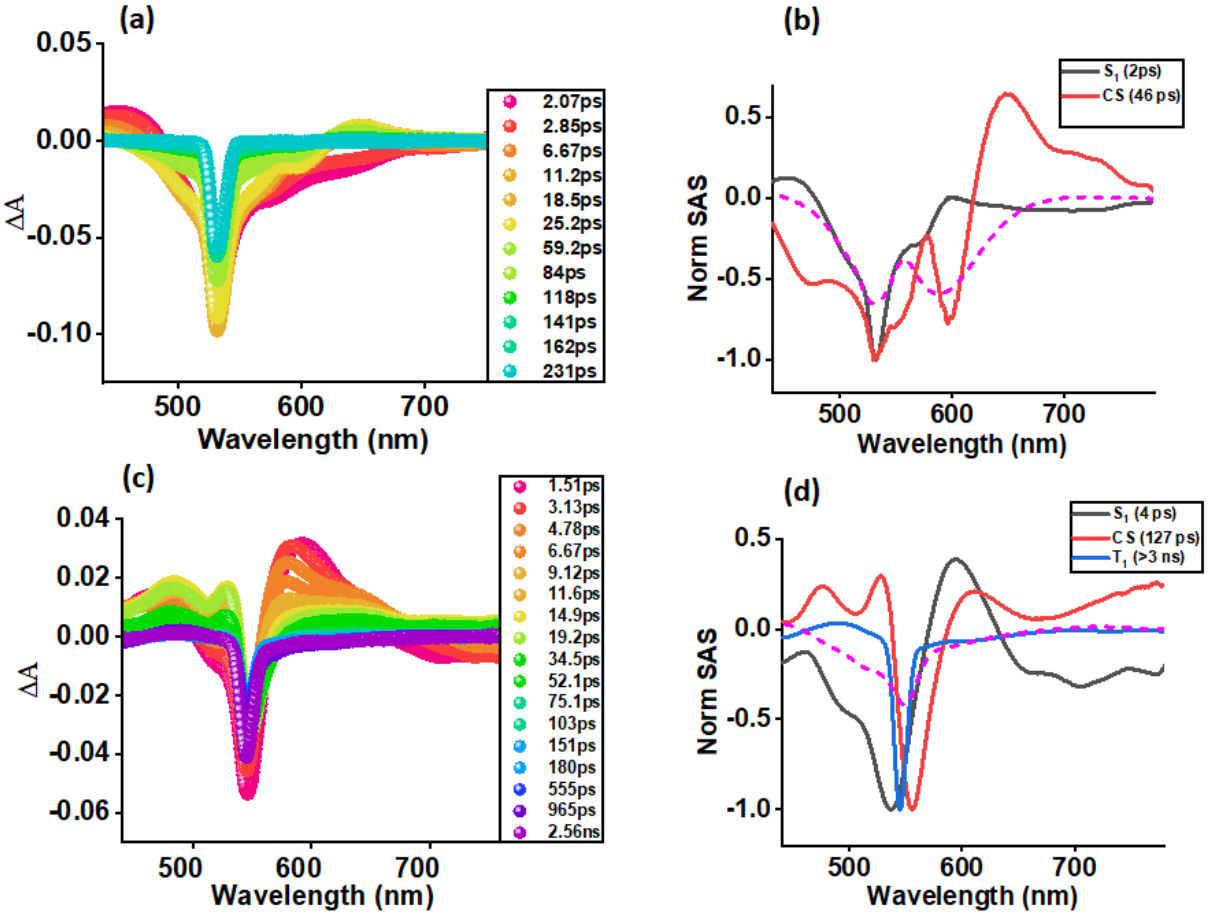

Figure 9. Fs-TA spectra at the indicated delay times of (a) **BODIPY 1** and (c) **BODIPY 2** excited at 536 nm and 550 nm, respectively in DCB. The species associated spectra from GloTarAn analysis of the transient data is shown for **BODIPY 1** and **BODIPY 2** in Figures b and d, respectively. The spectrum obtained by digitally combining the cation and anion spectrum minus neutral molecule representing the spectrum of the charge separated product is shown in Figures b and d by dash-dash lines.

fitting two components $S_1 \rightarrow CS \rightarrow GS$. The obtained lifetimes for S_1 and CS were 4 ps and 175 ps, respectively. Figure 9c depicts the femtosecond transient absorption spectra for **BODIPY 2**, excited state absorption (ESB) peaks were witnessed at 484, 529, and 586 nm, by comparing this spectrum to spectral changes during the first oxidation, the peak at 484 nm was assigned to the charge-separated state. Eventually, this charge-separated state is recombined to produce a triplet state. Whereas the peak at 586 nm could be attributed to the instant formation of $^1BODIPY^*$. One negative peak was also observed at 545 nm corresponding to GSB. Similarly, to **BODIPY 1**, the data was further evaluated by GloTarAn by fitting a simple three-component model $S_1 \rightarrow CS \rightarrow T_1 \rightarrow GS$ which resulted in generating SAS (Figure 9d) with lifetime values of 4 ps, 127 ps and >3 ns for S_1, CS, and T_1, respectively. And spectral characteristics of the dash-dash line are resembling CS from SAS, favoring the formation of charge separated species in **BODIPYs 1** and **2.**

Figure 10 shows the femtosecond transient absorption spectra for **BODIPYs 3–4** along with SAS at indicated delay times in dichlorobenzene solvent. In case of **BODIPY 3**, after exciting at 560 nm, ESA peak was observed at 650 nm which could be attributed to charge separation state by comparing to spectral changes during the first oxidation and reduction processes as shown in Figure 7c. In addition, two negative peaks were observed at 471, 556 nm which could be attributed to GSB by comparing with ground state absorbance. The data was further analyzed by GloTarAn by fitting a simple two component model $S_1 \rightarrow CS \rightarrow GS$ (this indicates CS state directly relaxing back to the ground state instead of populating long lived triplet state) to generate species associated spectra as shown in Figure 10b. This fit generated the lifetime values of 3 ps and 141 ps for S_1 and CS, respectively. The dash line in Figure 10b shows the spectrum of charge separated product, which was generated from spectroelectrochemical data by digitally merging the cation and anion spectrums minus neutral molecule. And its spectral characteristics are resembling CS from SAS, assisting the formation of charge separated species in **BODIPY 3**. Figure 10c represents the fs-TA for **BODIPY 4** after exciting at 560 nm with ESA peaks at 478 and 740 nm. The peak at 478 nm could be referred to instant formation of $^1BODIPY^*$ in first 3 ps after exciting, this peak then decayed and blue shifted, forming a new peak at 463 nm associated with charge transfer state, further rapid decaying and blue shifting of this peak, resulting in generating a new peak at 454 nm which could be ascribed to charge separated state as shown in above energy profile diagram in Figure 6. Due to GSB, a negative was also seen at 556 nm because of GSB. After fitting the three

components model $S_1 \rightarrow CT \rightarrow CS \rightarrow GS$ to the data, GloTarAn performed additional analysis on the data. Figure 10d presents the SAS findings of this analysis, which show lifetime values of 2 ps, 20 ps, and 159 ps for S_1, CS, and CS, respectively. And spectral characteristics of dash-dash line are resembling CS from SAS, assisting the formation of charge separated species in **BODIPY 4**.

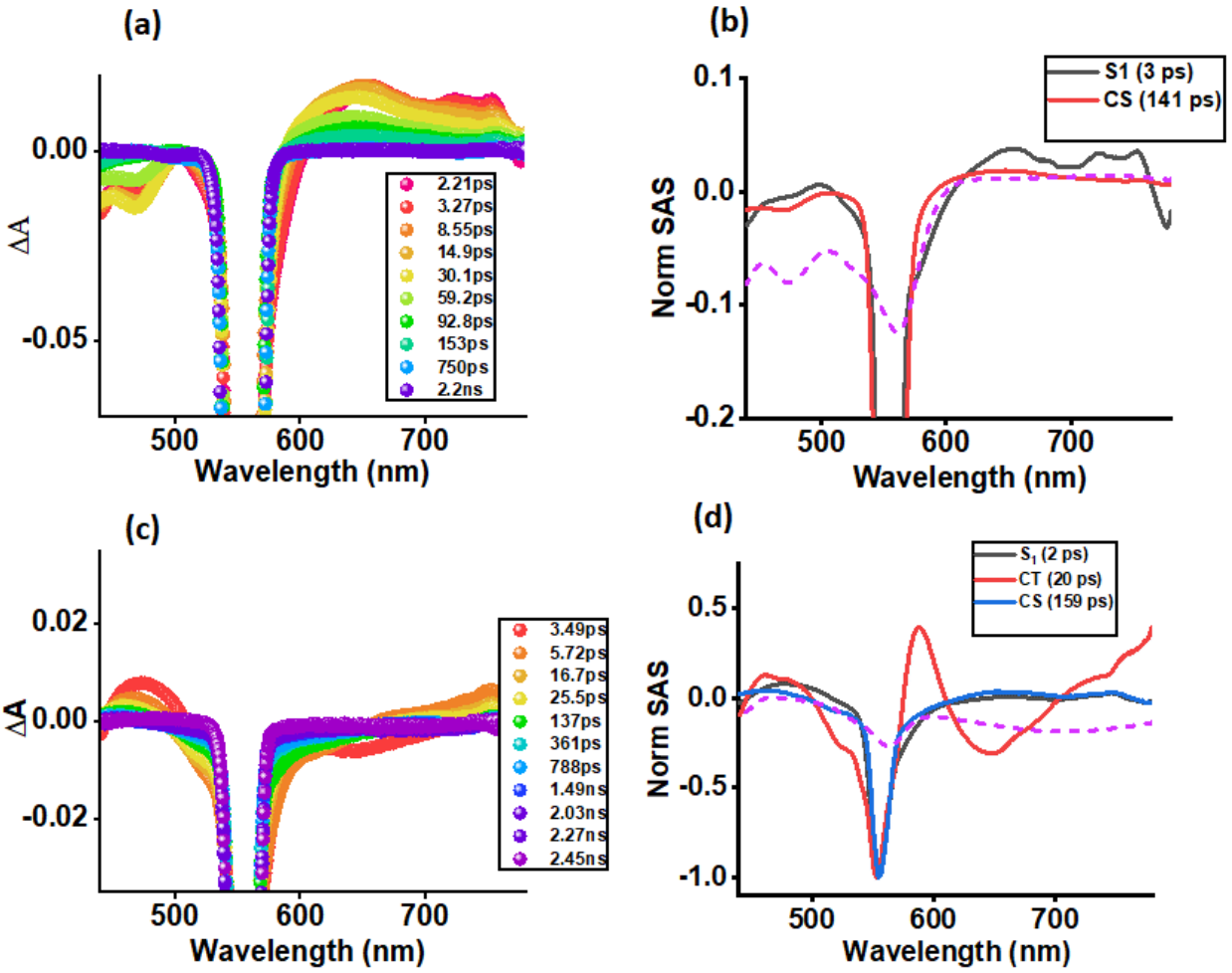

Figure 10. Fs-TA spectra at the indicated delay times of (a) **BODIPY 3** and (c) **BODIPY 4** excited at 560 nm, respectively in DCB. The species associated spectra from GloTarAn Analysis of the transient data is shown for **BODIPY 3** and **BODIPY 4** in Figures b and d, respectively. The spectrum obtained by digitally combining the cation and anion spectrum minus neutral molecule representing the spectrum of the charge separated product is shown in Figures b and d by the-dash lines.

CONCLUSIONS

In summary, a set of donor–acceptor (D–A) based **BODIPYs 1–4** were designed and synthesized *via* palladium-catalyzed Sonogashira cross-coupling and subsequent [2+2] cycloaddition-retroelectrocyclization reactions. The photophysical properties reveal that the **BODIPY 4** exhibits a strong ICT band at a longer wavelength region due to strong donor–acceptor interaction. The redox properties of push–pull **BODIPYs 1–4** exhibits multiple reduction waves due to presence of multiple-redox active entities. The **BODIPYs 3** and **4** exhibit multiple reduction waves at low potential as compared to **BODIPYs 1** and **2** due presence of strong acceptor groups. The theoretical results reveal that the incorporation of phenyl spacer, TCBD, and DCNQ units perturbs the HOMO–LUMO gap. The push–pull **BODIPYs 1–4** shows that the HOMOs are delocalized on both donor and acceptor BODIPY unit, whereas the LUMOs are localized on acceptor TCBD and DCNQ units. The **BODIPY 4** exhibits low HOMO–LUMO gap compared to **BODIPY 3** due to strong accepting nature of DCNQ unit. This report provides an important route for synthesizing a push–pull chromophores with low HOMO–LUMO gap for optoelectronic applications. Eventually, the femtosecond pump-probe was performed and it revealed the excited state charge separation (CS) process in dichlorobenzene for newly synthesized BODIPYs **1–4**. After analyzing fs-TA data by GloTarAn, the lifetime values were found in the range of 45–160 ps for these push-pull systems.

ASSOCIATED CONTENT

Supporting Information

The Supporting Information is available free of charge at https://pubs.acs.org/doi/xxxx.

Experimental Section and ^{1}H NMR, ^{13}C NMR, and HRMS spectra of all BODIPY derivatives, cyclic voltammograms, and computational results.

AUTHOR INFORMATION

Corresponding Authors

Rajneesh Misra

Department of Chemistry, Indian Institute of Technology, Indore 453552, India; orcid.org/0000-0003-3225-2125; Email: rajneeshmisra@iiti.ac.in

Francis D'Souza

Department of Chemistry, University of North Texas, 1155 Union Circle, #305070, Denton, TX 76203-5017, USA, orcid.org/0000-0003-3815-8949, E-mail: Francis.DSouza@UNT.edu

Authors

Indresh S. Yadav

Department of Chemistry, Indian Institute of Technology, Indore 453552, India

Ram R. Kaswan

Department of Chemistry, University of North Texas, 1155 Union Circle, #305070, Denton, TX 76203-5017, USA

Anuradha Liyanage

Department of Chemistry, University of North Texas, 1155 Union Circle, #305070, Denton, TX 76203-5017, USA

Conflict of Interest

There are no conflicts to declare.

Author Contributions

ISY, RRK, and AL contributed equally to this work.

ACKNOWLEDGMENT

We acknowledge the support of the US National Science Foundation (Grant No. 2000988 to FD), Council of Scientific and Industrial Research (Project No. 01/3112/23/EMR-II), Science and Engineering Research Board (SERB) projects CRG/2022/000023 and STR/2022/000001, New Delhi. We are grateful to the DST-FIST grant for the 500 MHz NMR facility and the Sophisticated Instrumentation Centre (SIC), Indian Institute of Technology (IIT) Indore.

REFERENCES

(1) Li, G.; Chen, Y.; Qiao, Y.; Lu, Y.; Zhou, G. Charge Transfer Switching in Donor–Acceptor Systems Based on BN-Fused Naphthalimides. *J. Org. Chem.* **2018**, *83* (10), 5577–5587.

(2) Larsen, C. B.; van der Salm, H.; Shillito, G. E.; Lucas, N. T.; Gordon, K. C. Tuning the Rainbow: Systematic Modulation of Donor–Acceptor Systems through Donor Substituents and Solvent. *Inorg. Chem.* **2016**, *55* (17), 8446–8458.

(3) McLay, J. R. W.; Sutton, J. J.; Shillito, G. E.; Larsen, C. B.; Huff, G. S.; Lucas, N. T.; Gordon, K. C. Transitioning from Intraligand π–π* to Charge-Transfer Excited States Using Thiophene-Based Donor–Acceptor Systems. *Inorg. Chem.* **2021**, *60* (1), 130–139.

(4) Pop, F.; Riobé, F.; Seifert, S.; Cauchy, T.; Ding, J.; Dupont, N.; Hauser, A.; Koch, M.; Avarvari, N. Tetrathiafulvalene-1,3,5-Triazines as (Multi)Donor–Acceptor Systems with Tunable Charge Transfer: Structural, Photophysical, and Theoretical Investigations. *Inorg. Chem.* **2013**, *52* (9), 5023–5034.

(5) Mandal, A. Tuning P-Type to n-Type Semiconductor Nature by Charge Transfer Cocrystallization: Effect of Transfer Integral vs. Reorganization Energy. *CrystEngComm* **2022**, *24* (11), 2072–2080.

(6) Gautam, P.; Misra, R.; Thomas, M. B.; D'Souza, F. Ultrafast Charge-Separation in Triphenylamine-BODIPY-Derived Triads Carrying Centrally Positioned, Highly Electron-Deficient, Dicyanoquinodimethane or Tetracyanobutadiene Electron-Acceptors. *Chem. – Eur. J.* **2017**, *23* (38), 9192–9200.

(7) Poddar, M.; Sharma, V.; Mobin, S. M.; Misra, R. 1,8-Naphthalimide-Substituted BODIPY Dyads: Synthesis, Structure, Properties, and Live-Cell Imaging. *Chem. – Asian J.* **2018**, *13* (19), 2881–2890.

(8) Washburn, S.; Kaswan, R. R.; Shaikh, S.; Moss, A.; D'Souza, F.; Wang, H. Excited-State Charge Transfer in Push–Pull Platinum(II) π-Extended Porphyrins Fused with Pentacenequinone. *J. Phys. Chem. A* **2023**, *127* (43), 9040–9051.

(9) Follana-Berná, J.; Dawson, A.; Kaswan, R. R.; Seetharaman, S.; Karr, P. A.; Sastre-Santos, Á.; D'Souza, F. π-Extended Pyrazinepyrene-Fused Zinc Phthalocyanines: Synthesis and Excited-State Charge Separation Involving Coordinated C60. *J. Phys. Chem. A* **2023**, *127* (30), 6191–6203.

(10) Dhindsa, J. S.; Buguis, F. L.; Anghel, M.; Gilroy, J. B. Band Gap Engineering in Acceptor-Donor-Acceptor Boron Difluoride Formazanates. *J. Org. Chem.* **2021**, *86* (17), 12064–12074.

(11) Popere, B. C.; Della Pelle, A. M.; Thayumanavan, S. BODIPY-Based Donor–Acceptor π-Conjugated Alternating Copolymers. *Macromolecules* **2011**, *44* (12), 4767–4776.

(12) Carlotti, B.; Poddar, M.; Elisei, F.; Spalletti, A.; Misra, R. Energy-Transfer and Charge-Transfer Dynamics in Highly Fluorescent Naphthalimide–BODIPY Dyads: Effect of BODIPY Orientation. *J. Phys. Chem. C* **2019**, *123* (40), 24362–24374.

(13) Niu, S.; Ulrich, G.; Retailleau, P.; Ziessel, R. Regioselective Synthesis of 5-Monostyryl and 2-Tetracyanobutadiene BODIPY Dyes. *Org. Lett.* **2011**, *13* (19), 4996–4999.

(14) Kong, L.; Wong, H.-L.; Tam, A. Y.-Y.; Lam, W. H.; Wu, L.; Yam, V. W.-W. Synthesis, Characterization, and Photophysical Properties of Bodipy-Spirooxazine and -Spiropyran Conjugates: Modulation of Fluorescence Resonance Energy Transfer Behavior via Acidochromic and Photochromic Switching. *ACS Appl. Mater. Interfaces* **2014**, *6* (3), 1550–1562.

(15) Gomez-Duran, C. F. A.; Hu, R.; Feng, G.; Li, T.; Bu, F.; Arseneault, M.; Liu, B.; Peña-Cabrera, E.; Tang, B. Z. Effect of AIE Substituents on the Fluorescence of Tetraphenylethene-Containing BODIPY Derivatives. *ACS Appl. Mater. Interfaces* **2015**, *7* (28), 15168–15176.

(16) Zatsikha, Y. V.; Didukh, N. O.; Swedin, R. K.; Yakubovskyi, V. P.; Blesener, T. S.; Healy, A. T.; Herbert, D. E.; Blank, D. A.; Nemykin, V. N.; Kovtun, Y. P. Preparation of Viscosity-Sensitive Isoxazoline/Isoxazolyl-Based Molecular Rotors and Directly Linked BODIPY–Fulleroisoxazoline from the Stable Meso-(Nitrile Oxide)-Substituted BODIPY. *Org. Lett.* **2019**, *21* (14), 5713–5718.

(17) Gao, H.; Gao, Y.; Wang, C.; Hu, D.; Xie, Z.; Liu, L.; Yang, B.; Ma, Y. Anomalous Effect of Intramolecular Charge Transfer on the Light Emitting Properties of BODIPY. *ACS Appl. Mater. Interfaces* **2018**, *10* (17), 14956–14965.

(18) Nguyen, V.-N.; Ha, J.; Koh, C. W.; Ryu, B.; Kim, G.; Park, J. H.; Kim, C.-Y.; Park, S.; Yoon, J. Access to the Triplet Excited States of Heavy-Atom-Free Boron-Dipyrromethene Photosensitizers via Radical Pair Intersystem Crossing for Image-Guided Tumor-Targeted Photodynamic Therapy. *Chem. Mater.* **2021**, *33* (19), 7889–7896.

(19) Misra, R.; Jadhav, T.; Dhokale, B.; Gautam, P.; Sharma, R.; Maragani, R.; Mobin, S. M. Carbazole-BODIPY Conjugates: Design, Synthesis, Structure and Properties. *Dalton Trans.* **2014**, *43* (34), 13076–13086.

(20) Shinde, J.; Thomas, M. B.; Poddar, M.; Misra, R.; D'Souza, F. Does Location of BF2-Chelated Dipyrromethene (BODIPY) Ring Functionalization Affect Spectral and Electron Transfer Properties? Studies on α-, β-, and Meso-Functionalized BODIPY-Derived Donor–Acceptor Dyads and Triads. *J. Phys. Chem. C* **2021**, *125* (43), 23911–23921.

(21) Gapare, R. L.; Thompson, A. Substitution at Boron in BODIPYs. *Chem. Commun.* **2022**, *58* (53), 7351–7359.

(22) Kumar, B.; Bhatta, A.; Saraf, P.; Rangan, K.; Sarkar, M.; Mitra, S.; Kumar, D. Iodine(III)-Promoted Regioselective and Efficient Synthesis of β-Triazolyl BODIPYs for the Selective Recognition of Nickel Ions and Bovine Serum Albumin. *Dalton Trans.* **2022**, *51* (21), 8169–8176.

(23) Lu, P.; Chung, K.-Y.; Stafford, A.; Kiker, M.; Kafle, K.; Page, Z. A. Boron Dipyrromethene (BODIPY) in Polymer Chemistry. *Polym. Chem.* **2021**, *12* (3), 327–348.

(24) Nenavath, S.; Duvva, N.; Kaswan, R. R.; Lim, G. N.; D'Souza, F.; Giribabu, L. Intramolecular Photoinduced Energy and Electron Transfer Reactions in Phenanthroimidazole–Boron Dipyromethane Donor–Acceptor Dyads. *J. Phys. Chem. A* **2023**, *127* (32), 6779–6790.

(25) Chong, H.; Lin, H.-A.; Shen, M.-Y.; Liu, C.-Y.; Zhao, H.; Yu, H. Step-Economical Syntheses of Functional BODIPY-EDOT π-Conjugated Materials through Direct C–H Arylation. *Org. Lett.* **2015**, *17* (13), 3198–3201.

(26) Kaneza, N.; Zhang, J.; Liu, H.; Archana, P. S.; Shan, Z.; Vasiliu, M.; Polansky, S. H.; Dixon, D. A.; Adams, R. E.; Schmehl, R. H.; Gupta, A.; Pan, S. Electrochemical and Spectroscopic Properties of Boron Dipyrromethene–Thiophene–Triphenylamine-Based Dyes for Dye-Sensitized Solar Cells. *J. Phys. Chem. C* **2016**, *120* (17), 9068–9080.

(27) Duan, C.; Zhou, Y.; Shan, G.-G.; Chen, Y.; Zhao, W.; Yuan, D.; Zeng, L.; Huang, X.; Niu, G. Bright Solid-State Red-Emissive BODIPYs: Facile Synthesis and Their High-Contrast Mechanochromic Properties. *J. Mater. Chem. C* **2019**, *7* (12), 3471–3478.

(28) Obondi, C. O.; Lim, G. N.; Karr, P. A.; Nesterov, V. N.; D'Souza, F. Photoinduced Charge Separation in Wide-Band Capturing, Multi-Modular Bis(Donor Styryl)BODIPY–Fullerene Systems. *Phys. Chem. Chem. Phys.* **2016**, *18* (27), 18187–18200.

(29) Filatov, M. A.; Karuthedath, S.; Polestshuk, P. M.; Callaghan, S.; Flanagan, K. J.; Telitchko, M.; Wiesner, T.; Laquai, F.; Senge, M. O. Control of Triplet State Generation in Heavy Atom-Free BODIPY–Anthracene Dyads by Media Polarity and Structural Factors. *Phys. Chem. Chem. Phys.* **2018**, *20* (12), 8016–8031.

(30) Wei, Z.; Sharma, S.; Philip, A. M.; Sengupta, S.; Grozema, F. C. Excited State Dynamics of BODIPY-Based Acceptor–Donor–Acceptor Systems: A Combined Experimental and Computational Study. *Phys. Chem. Chem. Phys.* **2021**, *23* (14), 8900–8907.

(31) Thompson, B. L.; Kieffer, I. A.; Heiden, Z. M. Utilization of BODIPY-Based Redox Events to Manipulate the Lewis Acidity of Fluorescent Boranes. *Chem. Commun.* **2022**, *58* (16), 2646–2649.

(32) Misra, R.; Dhokale, B.; Jadhav, T.; Mobin, S. M. The Quenching of Fluorescence as an Indicator of Donor-Strength in Meso Arylethynyl BODIPYs. *Dalton Trans.* **2014**, *43* (12), 4854–4861.

(33) Poddar, M.; Misra, R. NIR-Absorbing Donor–Acceptor Based 1,1,4,4-Tetracyanobuta-1,3-Diene (TCBD)- and Cyclohexa-2,5-Diene-1,4-Ylidene-Expanded TCBD-Substituted Ferrocenyl Phenothiazines. *Chem. – Asian J.* **2017**, *12* (22), 2908–2915.

(34) Patil, Y.; Popli, C.; Misra, R. Near-Infrared Absorbing Tetracyanobutadiene-Bridged Diketopyrrolopyrroles. *New J. Chem.* **2018**, *42* (5), 3892–3899.

(35) Misra, R.; Jadhav, T.; Nevonen, D.; Monzo, E. M.; Mobin, S. M.; Nemykin, V. N. Synthesis, Structures, and Redox Properties of Tetracyano-Bridged Diferrocene Donor–Acceptor–Donor Systems. *Organometallics* **2017**, *36* (22), 4490–4498.

(36) Zhang, Z.; Gou, G.; Wan, J.; Li, H.; Wang, M.; Li, L. Synthesis, Structure, and Significant Energy Gap Modulation of Symmetrical Silafluorene-Cored Tetracyanobutadiene and Tetracyanoquinodimethane Derivatives. *J. Org. Chem.* **2022**, *87* (5), 2470–2479.

(37) Khan, F.; Jang, Y.; Patil, Y.; Misra, R.; D'Souza, F. Photoinduced Charge Separation Prompted Intervalence Charge Transfer in a Bis(Thienyl)Diketopyrrolopyrrole Bridged Donor-TCBD Push-Pull System. *Angew. Chem.* **2021**, *133* (37), 20681–20690.

(38) Shoji, T.; Maruyama, M.; Shimomura, E.; Maruyama, A.; Ito, S.; Okujima, T.; Toyota, K.; Morita, N. Synthesis, Properties, and Redox Behavior of Tetracyanobutadiene and Dicyanoquinodimethane Chromophores Bearing Two Azulenyl Substituents. *J. Org. Chem.* **2013**, *78* (24), 12513–12524.

(39) Banziger, S. D.; Clendening, R. A.; Oxley, B. M.; Ren, T. Spectroelectrochemical and Computational Analysis of a Series of Cycloaddition–Retroelectrocyclization-Derived Donor–Acceptor Chromophores. *J. Phys. Chem. B* **2020**, *124* (52), 11901–11909.

(40) Rout, Y.; Gautam, P.; Misra, R. Unsymmetrical and Symmetrical Push–Pull Phenothiazines. *J. Org. Chem.* **2017**, *82* (13), 6840–6845.

(41) Yadav, I. S.; Alsaleh, A. Z.; Misra, R.; D'Souza, F. Charge Stabilization via Electron Exchange: Excited Charge Separation in Symmetric, Central Triphenylamine Derived, Dimethylaminophenyl–Tetracyanobutadiene Donor–Acceptor Conjugates. *Chem. Sci.* **2021**, *12* (3), 1109–1120.

(42) Finke, A. D.; Dumele, O.; Zalibera, M.; Confortin, D.; Cias, P.; Jayamurugan, G.; Gisselbrecht, J.-P.; Boudon, C.; Schweizer, W. B.; Gescheidt, G.; Diederich, F. 6,6-Dicyanopentafulvenes: Electronic Structure and Regioselectivity in [2 + 2] Cycloaddition–Retroelectrocyclization Reactions. *J. Am. Chem. Soc.* **2012**, *134* (43), 18139–18146.

(43) Dengiz, C.; Breiten, B.; Gisselbrecht, J.-P.; Boudon, C.; Trapp, N.; Schweizer, W. B.; Diederich, F. Synthesis and Optoelectronic Properties of Janus-Dendrimer-Type Multivalent Donor–Acceptor Systems. *J. Org. Chem.* **2015**, *80* (2), 882–896.

(44) Li, Y.; Tsuboi, K.; Michinobu, T. Double Click Synthesis and Second-Order Nonlinearities of Polystyrenes Bearing Donor−Acceptor Chromophores. *Macromolecules* **2010**, *43* (12), 5277–5286.

(45) Shoji, T.; Miura, K.; Araki, T.; Maruyama, A.; Ohta, A.; Sekiguchi, R.; Ito, S.; Okujima, T. Synthesis of 2-Methyl-1-Azulenyl Tetracyanobutadienes and Dicyanoquinodimethanes: Substituent Effect of 2-Methyl Moiety on the Azulene Ring toward the Optical and Electrochemical Properties. *J. Org. Chem.* **2018**, *83* (12), 6690–6705.

(46) Philippe, C.; Bui, A. T.; Batsongo-Boulingui, S.; Pokladek, Z.; Matczyszyn, K.; Mongin, O.; Lemiègre, L.; Paul, F.; Hamlin, T. A.; Trolez, Y. 1,1,4,4-Tetracyanobutadiene-Functionalized Anthracenes: Regioselectivity of Cycloadditions in the Synthesis of Small Near-IR Dyes. *Org. Lett.* **2021**, *23* (6), 2007–2012.

(47) Kraußе, N.; Kielmann, M.; Ma, J.; Butenschön, H. Reactions of Alkynyl- and 1,1′-Dialkynylferrocenes with Tetracyanoethylene – Unanticipated Addition at the Less Electron-Rich of Two Triple Bonds. *Eur. J. Org. Chem.* **2015**, *2015* (12), 2622–2631.

(48) Yadav, I. S.; Jang, Y.; Rout, Y.; Thomas, M. B.; Misra, R.; D'Souza, F. Near-IR Intramolecular Charge Transfer in Strongly Interacting Diphenothiazene-TCBD and Diphenothiazene-DCNQ Push-Pull Triads. *Chem. – Eur. J.* **2022**, *28* (25), e202200348.

(49) Poddar, M.; Jang, Y.; Misra, R.; D'Souza, F. Excited-State Electron Transfer in 1,1,4,4-Tetracyanobuta-1,3-Diene (TCBD)- and Cyclohexa-2,5-Diene-1,4-Diylidene-Expanded TCBD-Substituted BODIPY-Phenothiazine Donor–Acceptor Conjugates. *Chem. – Eur. J.* **2020**, *26* (30), 6869–6878.

(50) Gautam, P.; Dhokale, B.; Mobin, S. M.; Misra, R. Ferrocenyl BODIPYs: Synthesis, Structure and Properties. *RSC Adv.* **2012**, *2* (32), 12105–12107.

(51) Dhokale, B.; Jadhav, T.; Mobin, S. M.; Misra, R. Tetracyanobutadiene Functionalized Ferrocenyl BODIPY Dyes. *Dalton Trans.* **2016**, *45* (4), 1476–1483.

Table of contents